Article

Steric Effects in Electron Transfer from Potassium to π-Bonded Oriented Molecules CHCN, CHNC, and CClCN

Philip R. Brooks, Peter W. Harland, Sean A. Harris, Terry Kennair, Crystal Redden, and Jack F. Tate

J. Am. Chem. Soc., **2007**, 129 (50), 15572-15580 • DOI: 10.1021/ja074302d

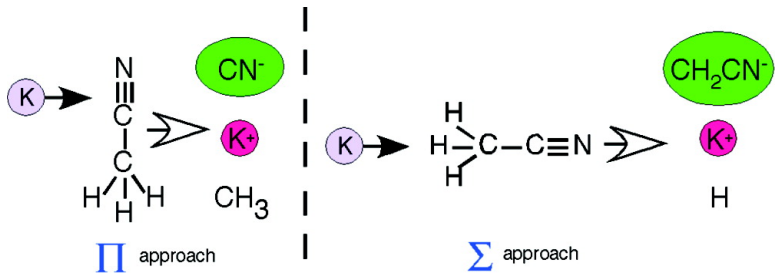

More About This Article

Additional resources and features associated with this article are available within the HTML version:

- Supporting Information
- Access to high resolution figures
- Links to articles and content related to this article
- Copyright permission to reproduce figures and/or text from this article

View the Full Text HTML

J|A|C|S
ARTICLES
Published on Web 11/28/2007

Steric Effects in Electron Transfer from Potassium to π-Bonded Oriented Molecules CH_3CN, CH_3NC, and CCl_3CN

Philip R. Brooks,* Peter W. Harland,† Sean A. Harris, Terry Kennair, Crystal Redden, and Jack F. Tate

Contribution from the Chemistry Department and Rice Quantum Institute, Rice University, Houston, Texas 77251

Received June 13, 2007; E-mail: brooks@python.rice.edu

Abstract: Electron transfer from K atoms to oriented CH_3CN, CH_3NC, and CCl_3CN is studied in crossed beams at energies near the threshold for forming an ion pair. For the methyl compounds, the dominant ions are K^+ and CN^-; the steric asymmetry is very small and energy-independent, characteristic of sideways attack with the electron apparently entering the π^*_{CN} antibonding orbital. Migration of the electron to the σ^*_{CC} orbital to break the C−C bond is greatly facilitated by interaction with the atomic donor. CH_2CN^- is formed in collisions preferring CH_3-end attack, and the steric asymmetry becomes very large near threshold. CCl_3CN mostly forms Cl^- in collisions slightly favoring the CCl_3 end with a small energy dependence with the electron apparently entering the σ^* LUMO. CN^- is formed in much smaller yield with a slight preference for the CN end. The parent negative ion CCl_3CN^- is observed, and a lower limit for its electron affinity is estimated to be 0.3 eV. Fragment ions CCl_2CN^- and $ClCN^-$ are also observed with upper limits for the quantity bond dissociation energy − electron affinity (BDE − EA) estimated to be 0.6 and 1.0 eV, respectively.

1. Introduction

Electrons bind nuclei together into molecules, and chemical reactions are a consequence of rearrangement of electrons around the nuclei involved. The transfer of electrons is thus fundamental to chemistry, but since few reactions produce charged particles under normal conditions, the participation of the electron is only rarely evident, such as in reactions in electric cells. But even though electron-transfer reactions are often disguised, they still play a central role in chemistry and biochemistry.[1,2]

The electron-transfer event is not the transfer of a free electron, but rather a curve-crossing between different diabatic electronic states[3−5] approximately described by the Landau−Zener theory. For the case considered here, that theory considers the (avoided) crossing between a neutral diabatic potential energy curve and an ionic diabatic potential energy curve. The probability of an electron "jump" (actually an adiabatic transition from a neutral surface to an ionic surface) depends mainly on the species involved and their electronic potential surfaces. An electron may jump as the reagents approach or as the products recede. The overall probability can be very complex because molecules have many degrees of freedom, and if the electron jumps at the first crossing, as the products recede, the geometry of the molecule could be so different from the reagent geometry that the electron does not jump back.[6] (This has been called "bond stretching[7]" in simpler systems.) Without question, the electron-transfer process is a concerted event involving the properties of the donor and the acceptor.

Most chemical reactions lack the energy required to reach these curve crossings but occur in condensed phases because the solvent can act to activate the reagents and deactivate the product.[8] This further complicates the overall process. To directly examine the electron-transfer event itself and avoid the obfuscation of the solvent, we study electron transfer from isolated atoms to simple isolated molecules in crossed molecular beams at collision energies high enough to separately detect the positive and negative ions formed by the electron transfer. This is still a concerted process, involving both the donor and the acceptor and their interaction but without the solvent. In contrast, *free* electrons can also interact with molecules in attachment processes that involve only the acceptor and are therefore not concerted reactions.[9] Interactions with *free* electrons are of particular interest in studying the effects of radiation damage[10−12] but are not directly related to the problem of electron transfer.

At energies close to the threshold for separating ions, the electron must be captured in the molecular LUMO, but the fate of the (probably unstable) transient negative ion depends on

† Present address: Chemistry Department, University of Canterbury, Christchurch, New Zealand.

(1) Ashby, E. C. *Acc. Chem. Res.* **1988**, *21*, 414−21.
(2) Rossi, R. A.; Pierini, A. B.; Penenory, A. B. *Chem. Rev.* **2003**, 71−167.
(3) Baede, A. P. M. *Adv. Chem. Phys.* **1975**, *30*, 463−535.
(4) Kleyn, A. W.; Los, J.; Gislason, E. A. *Phys. Rep.* **1982**, *90*, 1−71.
(5) Kleyn, A. W.; Moutinho, A. M. C. *J. Phys. B: At. Mol. Opt. Phys.* **2001**, *34*, R1−44.
(6) Harland, P. W.; Carman, H. S.; Phillips, L. F.; Brooks, P. R. *J. Chem. Phys.* **1990**, *93*, 1089−1097.
(7) Hubers, M. M.; Los, J. *Chem. Phys.* **1975**, *10*, 235−259.
(8) Marcus, R. A.; Sutin, N. *Biochim. Biophys. Acta* **1985**, *811*, 265−322.
(9) Illenberger, E.; Momigny, J. *Gaseous Molecular Ions*; Springer-Verlag: New York, 1992.

10.1021/ja074302d CCC: $37.00

the presence or absence of the donor,[13] and different products often result for the two processes. In the present experiments, we probe not only the identity of the negative ions produced but also how those ions depend on the initial orientation of the molecular target.

Previous studies concerning the orientation have mainly involved small alkyl halide molecules[14−18] where the LUMO is expected to be a σ^* orbital and occupation of that orbital could easily cause bond rupture. The effect of orientation for several small molecules such as CH_3Br was large although unfavorable orientation could be overcome with enough collision energy. In some instances, the favorable orientation in these σ-bonded molecules changed at very low energy to better enable the product ions to separate.[16,17] It would clearly be of interest to examine how the orientation requirements in σ-bonded molecules compare with those in π-bonded molecules, but our method of orientation requires symmetric-top molecules having dipole moments along the C_{3v} symmetry axis, ruling out studies on everybody's choice, benzene.

Acetonitrile, CH_3NC, and CCl_3CN are symmetric tops with large dipole moments that can be oriented, and the present experiments on the nitriles and isonitriles were undertaken to assess the role, if any, played by π^* orbitals. For CH_3CN, preliminary experiments showed that CN^- and CH_2CN^- were preferentially formed in attacks at the CN and CH_3 ends of the molecule, respectively. The steric asymmetry was small (as were the signals), and we suggested that CN^- possibly favored sideways attack. The S/N in the present experiments is much larger, and the steric asymmetry has been measured for both ions at energies near the threshold for ion-pair formation. We find copious amounts of CN^- produced with near-zero steric asymmetry independent of energy over a 6 eV range above the threshold for ion-pair formation. This behavior is qualitatively different from the alkyl halides, and shows that CN^- acts as more than a "super halogen". We believe that CN^- is produced mainly in sideways attack of the π^* orbital. To form CN^-, the CH_3-CN bond must be broken by transferring the π^* electron to the σ^* orbital, and this transfer and subsequent bond rupture is apparently facilitated by a concerted interaction with the K ion. (For the attachment of free electrons, there is no $\pi^*-\sigma^*$ transfer and CN^- is a minor product.[19,20]) Smaller amounts of CH_2CN^- are formed favoring CH_3-end attack, probably into the σ^*_{CH} LUMO+1. The steric properties of CH_3NC are similar to those of CH_3CN. For CCl_3CN, the products are more varied and consistent with the LUMO being the σ^*_{CCl} orbital.

2. Experimental Section

An atomic beam of hyperthermal potassium atoms intersects a beam of oriented molecules midway between two time-of-flight (TOF) mass spectrometers and ions formed in the electron-transfer collision are detected and counted in coincidence.

Fast neutral atoms are produced by first surface ionizing atoms on biased rhenium or tungsten wires and then accelerating the ions through a grounded slit into a field-free region inside the oven containing the atomic vapor. Resonant charge-exchange collisions between ions and neutral atoms occur as the ions drift through the vapor, producing a beam of fast neutrals. Any residual ions are deflected out of the beam by charged plates. The resulting beam of fast atoms passes through a heated skimmer, through a separate ultrahigh vacuum (uhv) chamber and is dumped in a separate differentially pumped chamber.[14,15,21,22]

The fast K beam crosses a seeded beam of CH_3CN, CH_3NC, or CCl_3CN inside the uhv chamber midway between the TOF spectrometers. Gas beams are produced by passing helium through a fiberglass sleeve immersed in one of the liquids thermostated at 0 °C where the vapor pressures were 24, 6, and 18 Torr, respectively. The total backing pressure was 150 Torr. Acetonitrile (ACS certified) and CCl_3CN (98% purity) were purchased from Fisher and Aldrich, respectively, and used without further purification. Methyl isocyanide, CH_3NC, was synthesized by standard techniques;[23] NMR analysis indicated pure CH_3NC with no traces of CH_3CN nor starting materials. All liquids were outgassed with standard freeze−thaw techniques.

The seeded gas beam travels through a 1.4 m hexapole electric field, through the uhv chamber, and is dumped in another separately pumped chamber. When high voltage (HV) is applied to the hexapole rods (typically ±10 kV), molecules in some quantum states are attracted to the rods and defocused, whereas molecules in other states are deflected toward the axis and increase the intensity of the beam.[24,25] These molecules are oriented in a (weak) electric field with $\langle\cos\theta\rangle = MK/[J(J+1)]$, where $\langle\cos\theta\rangle$ is the average of the cosine of the angle between the field and the top axis, and the quantum numbers J, K, and M correspond to the total angular momentum, its projection on the top axis, and its projection on the electric field, respectively.[26] This deflection in the hexapole field selects molecules with $MK < 0$, corresponding to molecules in "high-energy" orientations where the positive end of the molecule points toward a positively charged plate. The molecules are oriented with respect to the local electric field, which gradually changes from that inside the hexapole to the uniform field between the two TOF mass spectrometers. The orientation of the molecule at the collision region can be changed by reversing the direction of the field, which is accomplished by interchanging the polarities of the TOF mass spectrometers.

The beams are continuous and the TOF voltages are DC so there is no time zero for the TOF. But an electron-transfer simultaneously produces a K^+ ion and a negative ion of unknown mass, and the difference in flight times is a signature of the mass of the negative ion. The ions in each mass spectrometer are detected with multichannel plate (MCP) detectors. The pulse from the positive ion MCP starts a time-to-digital converter (TDC), and the pulse from the negative ion MCP (after a 4 μs delay to ensure that the positive pulse always arrives first) stops the digitizer. The time difference is read out by computer and the TDC is reset to await the next ion pair.

A computer acquires data and controls the experiment. For each energy of the atom chosen, coincidence TOF data are acquired for HV

(10) Scheer, A. M.; Mozejko, P.; Gallup, G. A.; Burrow, P. D. *J. Chem. Phys.* **2007**, *126*, 174301−174307.
(11) Baccarelli, I.; Gianturco, F. A.; Grandi, A.; Lucchese, R. R.; Sanna, N.; Bald, I.; Kopyra, J.; Illenberger, E. *J. Am. Chem. Soc.* **2007**, *129*, 6269−6277.
(12) Huber, D.; Beikircher, M.; Denifl, S.; Zappa, F.; Matejcik, S.; Bacher, A.; Grill, V.; Ma[uml]ark, T. D.; Scheier, P. *J. Chem. Phys.* **2006**, *124*, 084304.
(13) Nalley, S. J.; Compton, R. N.; Schweinler, H. C.; Anderson, V. E. *J. Chem. Phys.* **1973**, 4125−4144.
(14) Harris, S. A.; Wiediger, S. D.; Brooks, P. R. *J. Phys. Chem.* **1999**, *103*, 10035−10041.
(15) Harris, S. A.; Brooks, P. R. *J. Chem. Phys.* **2001**, *114*, 10569−10572.
(16) Brooks, P. R.; Harris, S. A. *J. Chem. Phys.* **2002**, *117*, 4220−4232.
(17) Jia, B.; Laib, J.; Lobo, R. F. M.; Brooks, P. R. *J. Am. Chem. Soc.* **2002**, *124*, 13896−13902.
(18) Harland, P. W.; Brooks, P. R. *J. Am. Chem. Soc.* **2003**, *125*, 13191−13197.
(19) Heni, M.; Illenberger, E. *Int. J. Mass Spectrom. Ion Processes* **1986**, *73*, 127−144.
(20) Sailer, W.; Pelc, A.; Limao-Vieira, P.; Mason, N. J.; Limtrakul, J.; Scheier, P.; Probst, M.; Mark, T. D. *Chem. Phys. Letters* **2003**, *381*, 216−222.
(21) Xing, G.; Kasai, T.; Brooks, P. R. *J. Am. Chem. Soc.* **1995**, *117*, 2581−2589.
(22) Harris, S. A.; Harland, P. W.; Brooks, P. R. *Phys. Chem. Chem. Phys.* **2000**, *2*, 787−791.
(23) Schuster, R. E.; Scott, J. E. J.; Casanova, J. *Org. Syn. Coll. Vol.* **1973**, *5*, 772−773.
(24) Brooks, P. R.; Jones, E. M.; Smith, K. *J. Chem. Phys.* **1969**, *51*, 3073−3081.
(25) Brooks, P. R. *Science* **1976**, *193*, 11−16.
(26) Townes, C. H.; Schawlow, A. L. *Microwave Spectroscopy*; Dover: New York, 1975.

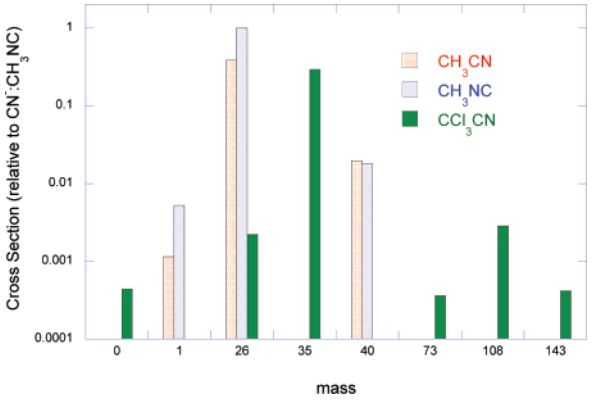

Figure 1. Cross sections relative to CN^- (CH_3NC) for forming various ions 3 eV above their respective thresholds. Note log scale.

on and HV off for positive-end approach and negative-end approach. The data acquired for HV off are from molecules that have not been state selected and are thus truly randomly oriented. These data are used to compare the sensitivities of the two MCP's. The energies are randomly varied to avoid systematic drifts.

3. Results

3.1. Mass Spectra. Mass spectra of the negative ions for acetonitrile, CH_3CN, and methyl isocyanide, CH_3NC are very similar, but these differed enormously from that for trichloroacetonitrile, CCl_3CN, and are shown in Figure 1 for illustration. Although the count rate depends on the intensity of each beam, this was relatively constant for each molecule from run to run. Assuming beam intensity is proportional to the vapor pressure, cross sections relative to CN^- from CH_3NC are evaluated from the average HV_{ON} signal 3 eV above each ion's threshold and plotted in Figure 1. Several points are apparent: whereas the cross section for forming CN^- is nearly the same for CH_3CN and CH_3NC, the cross section for forming CN^- from CCl_3CN is some *2* orders of magnitude smaller. The cross section for forming Cl^- from CCl_3CN is comparable to those for CN^- from CH_3CN/CH_3NC, and the cross sections for forming CH_2CN^- or CH_2NC^- are about equal. Other ions are clearly produced in far smaller concentration. Electron signals for acetonitrile and methyl isocyanide apparently arise only from some background process, as previously reported.[22]

3.2. Energy Calibration. To calibrate the collision energy, apparent laboratory thresholds were determined for each ion observed by plotting HV_{ON} and HV_{OFF} signals for positive end and negative end attack. The signal rates, *S*, for the various ions were fairly reproducible from day to day and these plots could be well-fit with a threshold and a quadratic for energies above threshold,

$$S = a\ (E < E_{th})$$

$$S = a + b(E - E_{th}) + c(E - E_{th})^2\ (E \geq E_{th}) \qquad (1)$$

where E is the accelerating voltage and E_{th} is the apparent threshold. Thresholds are usually identical for positive end and negative end attack and representative thresholds are shown in Figure 2.

For any given ion pair, there is a minimum threshold energy, E_{th}, required to separate the ions so that they can be detected,

$$E_{th} \geq \text{IP} + \text{BDE} - \text{EA} \qquad (2)$$

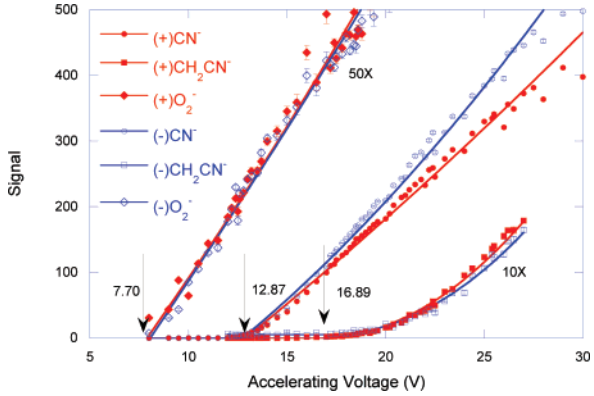

Figure 2. HV_{ON} signals from CH_3CN for positive-end and negative-end attack plotted *vs* accelerating voltage. Lines are quadratic fits above the threshold. O_2^- is observed as an impurity in CH_3CN and is not affected by the high voltage and the "positive" and "negative" fits are essentially coincident.

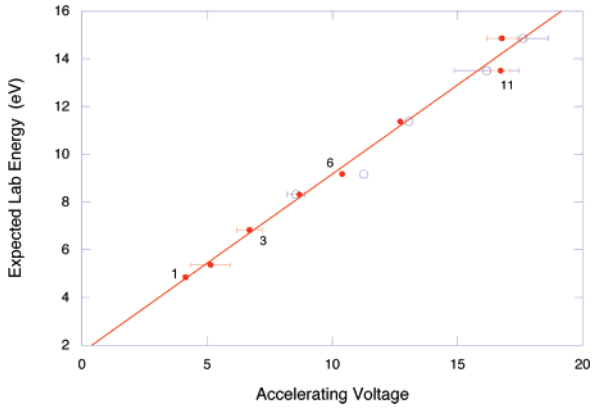

Figure 3. Expected lab energies calculated from Eq 2 and transformed into the laboratory *vs* experimental threshold voltages. Points numbered to represent ions (from molecules) 1:Cl^- (CCl_3CN), 2:e^- (CCl_3CN), 3:CN^- (CCl_3CN), 4:O_2^- (CH_3CN), 5:O_2^- (CH_3CN)[W], 6:CN^- (CH_3NC), 7:CN^- (CH_3NC)[W], 8:CN^- (CH_3CN), 9:CN^- (CH_3CN)[W], 10:CH_2CN^- (CH_3CN)[W], 11:CH_2CN^- (CH_3CN), 12:CH_2NC^- (CH_3NC), 13:CH_2NC^- (CH_3NC)[W]. Open points are obtained using atoms surface ionized on tungsten [W] filaments; all others ionized using rhenium. Calibration line is a least-square fit to all data.

where IP is the ionization energy of the alkali metal (K), EA the electron affinity of the species forming the negative ion, and BDE the bond dissociation energy of any bond that is broken. The inequality arises because one or more of the fragments could be excited. For various well-characterized ions (e^-, CN^-, CH_2CN^-, etc) thresholds could be calculated from values in the NIST webbook.[27] Others such as Cl^- from CCl_3CN relied upon bond dissociation energies estimated from related compounds.[28] The center-of-mass thresholds from eq 2 were transformed to laboratory collision energies and plotted vs the experimental voltage thresholds as shown in Figure 3. Laboratory energies are used for this plot to display thresholds for CCl_3CN as well as those from CH_3CN and CH_3NC. Using the calibration from Figure 3, we evaluate the corrected lab energy for each accelerating voltage, and from the corrected lab energy, we calculate the CM energy. This energy will be used in subsequent plots.

(27) NIST; NIST Standard Reference Database Number 69: 2003.
(28) Luo, Y.-R. *Handbook of Bond Dissociation Energies in Organic Compounds*; CRC Press: Boca Raton, 2003.

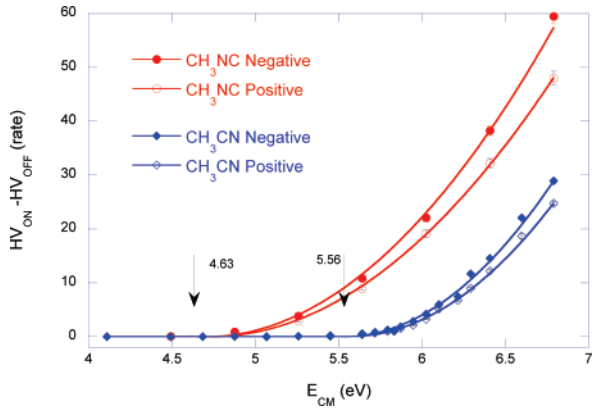

Figure 4. $HV_{ON}-HV_{OFF}$ signal rates *vs* energy for CN^- from CH_3NC (round points) and CH_3CN (diamonds). Curves are least square quadratic fits with the thresholds indicated.

3.3. CH_3CN and CH_3NC. Electron transfer to acetonitrile (CH_3CN) and methyl isocyanide (CH_3NC) is remarkably similar. Both molecules yield mainly CN^- with small amounts of CH_2CN^- and CH_2NC^- produced as the energy is increased. Very small signals corresponding to electrons and H^- are observed, but the H^- signal increases when the HV is applied whereas the electron signal does not. Since the HV focuses the symmetric top molecules, the beam intensity increases and the signals from reaction products involving the symmetric top molecule must also increase. The electrons observed are not from a molecule that focuses and are thus from some background process and not from CH_3CN. A signal from O_2^- is also frequently observed (and is also independent of the HV), apparently from oxygen not removed by the freeze−thaw cycles. The O_2^- signals were helpful for mass and energy calibration, and no effort was made to eliminate them.

Signals from CN^- require that the CH_3-CN or CH_3-NC bond be broken, and since these have different strengths, the CN^- thresholds are considerably different, as shown in Figure 4. The energy has been calibrated using the data in Figure 2, and the thresholds shown, 4.6_3 and 5.5_6 eV, differ slightly from the results calculated using the literature, 4.8_0 and 5.7_3, reflecting an uncertainty of ~0.2 eV in our energy calibration.

The signals shown in Figure 4 suggest that production of CN^- is favored for negative-end attack. Although this is true, the absolute signal (or difference here) also reflects swapping detectors to reverse the orienting electric field. We eliminate any detector bias by comparing signals obtained with the HV focusing field turned off: the molecules are truly randomly oriented when the HV is off and the signals are normalized to be identical.[16]

After normalizing the HV_{OFF} signals we evaluate the experimental steric asymmetry factor, defined as

$$G(E) = [\sigma_-(E) - \sigma_+(E)]/[\sigma_-(E) + \sigma_+(E)]$$

where $\sigma_\pm(E)$ is the energy-dependent cross section for attack at the positive or negative end of the molecule. The steric asymmetry factor for CN^- is shown in Figure 5 and that for CH_2CN^- is shown in Figure 6. For CN^- from CH_3CN the steric asymmetry is very small and slightly favors the CN end of the molecule. There is *no* dependence on energy, and the data for CH_3NC are scattered about the line through the CH_3CN data. (More data were taken with CH_3CN because it was readily

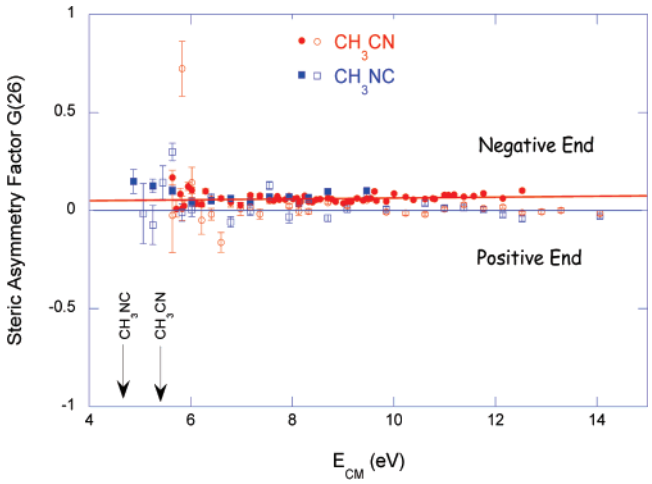

Figure 5. Steric asymmetry factor for producing CN^- from CH_3CN (red symbols) or from CH_3NC (blue squares). Filled symbols refer to data taken using a rhenium wire in the charge exchange oven, open symbols taken using a tungsten wire. Thresholds for the molecules are denoted by arrows. The line is a linear least-square fit through the CH_3CN data taken using a rhenium filament.

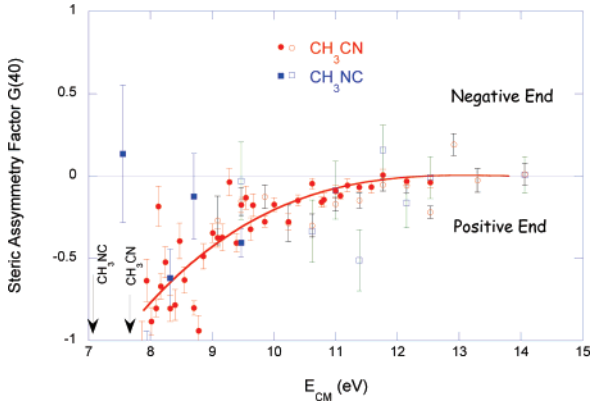

Figure 6. Steric asymmetry factor for producing CH_2CN^- from CH_3CN (red circles) or CH_3NC (blue squares). The thresholds are different and denoted by arrows. The curve is a smooth line drawn through the CH_3CN data taken with a rhenium filament and is included only to show trend.

available.) The small value of G and its apparent energy independence strongly suggests that sideways attack is preferred for producing CN^-.

The signals at $m/e = 40$, corresponding to CH_2CN^- are much smaller than those at $m/e = 26$ (CN^-), and the steric asymmetry is a bit more scattered, but Figure 6 shows that attack at the positive (CH_3) end of the molecule is clearly favored. The preference for CH_3-end attack is strongest at energies near threshold and fades to zero as the energy is increased.

The signals at $m/e = 1$ (H^-) are very small but clearly depend on the hexapole voltage so they arise from CH_3CN molecules. The steric asymmetry factor for H^- is scattered, but as shown in Figure 7 the steric asymmetry for H^- resembles that for forming CN^- and is different from that for CH_2CN^-, the complementary ion formed if the C−H bond is broken.

Figure 8 shows the average ion fractions $\bar{X} = (X_+ + X_-)/2$ as a function of energy, where $X_\pm$ denotes the fraction in the positive or negative orientation. (The average is used because a steric effect for any one ion affects all the fractions and would be misleading.) The signal at $m/e = 1$ (H^-) is typically ≪1% of the signal, and we were not able to determine the threshold very well. The threshold for producing CH_2CN^- is about 7.5

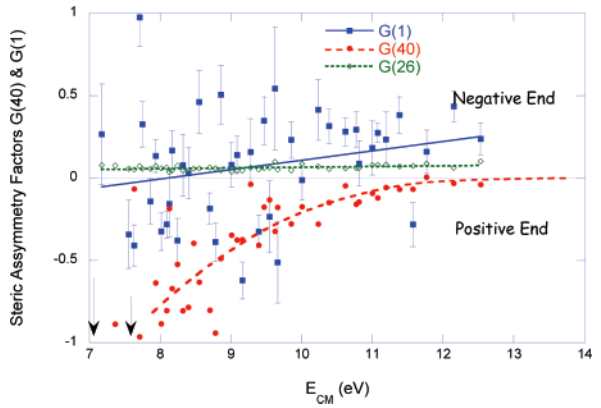

Figure 7. Steric asymmetry factors for forming H^- compared to those for forming CN^- or CH_2CN^-. The solid line is a linear least-square fit through the H^- data.

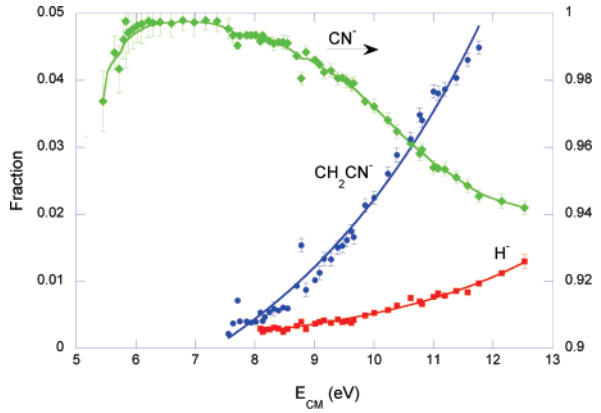

Figure 8. Average fraction of ions from CH_3CN *vs* collision energy. Smooth curves and some error bars are included for illustration. Right hand ordinate only for CN^-.

eV and as that ion (and also apparently the H^-) is formed, the fraction of CN^- produced begins the fall off.

3.4. CCl_3CN. Ions Formed. CCl_3CN is in many respects more interesting than CH_3CN/CH_3NC not only because the signal is higher at a given LAB energy, but also because more ionic species are formed. Negative ions were produced by CCl_3CN collisions at nominal values of m/e = 0, 26, 35, 73, 108, and 143, corresponding to the species e^-, CN^-, Cl^-, $ClCCN^-$, Cl_2CCN^-, and Cl_3CCN^- (the parent ion). The chlorine isotopes caused broadening of the mass peaks for all the Cl-containing species.

The fraction of ions observed as a function of energy (analogous to Figure 8 for CH_3CN) is shown in Figure 9. The dominant ion is clearly Cl^- rather than CN^- which is not surprising since the C−Cl bond is ∼2 eV weaker than the C−CN bond. (The electron affinity of CN is only slightly greater than that of Cl.) CN^- increases exponentially from a threshold near 5.5 eV, and the parent negative ion decays exponentially with energy as expected. The free electron is always a very small signal and it should be noted that it does not increase at the expense of the parent negative ion, so the parent ion is chemically decomposing rather than auto-detaching an electron. Cl_2CCN^- is present in appreciable concentrations and the energy dependence is unusual.

Threshold energies were determined (after energy calibration) for the electron and the ions CN^-, Cl^-, $ClCCN^-$, Cl_2CCN^-, and Cl_3CCN^-. The experimental and theoretical thresholds for

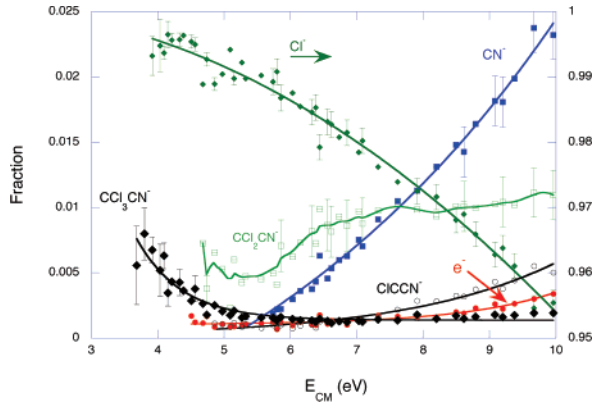

Figure 9. Average ion fraction for various ions resulting from electron transfer from K atoms to CCl_3CN. Smooth curves are passed through the experimental points for visual clarity. Right hand ordinate applies only to Cl^-.

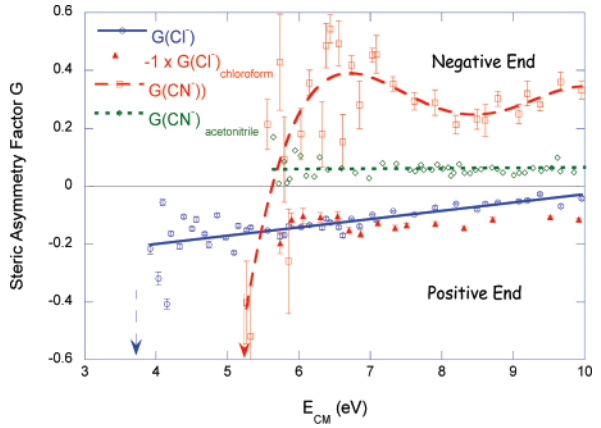

Figure 10. Steric asymmetry factors for formation of Cl^- and CN^- on electron transfer from potassium to CCl_3CN. Line through Cl^- data is a linear least-square fit, that through CN^- is for illustration. Arrows denote thresholds. Dotted line is for $G(CN^-)$ for acetonitrile from Figure 5. Diamonds are $-1 \times G(Cl^-)$ for CCl_3H from ref 17.

Table 1. Threshold Energies and Deduced Parameters[a]

species	threshold ± 0.2 eV	(BDE − EA) eV
$ClCCN^-$	5.37	≤1.0
Cl_2CCN^-	4.98	≤0.6

[a] IP(K) = 4.34 eV, reference 27.

the electron, CN^- and Cl^- agree reasonably well but they were used for calibration. Three of the ions, $ClCCN^-$, Cl_2CCN^-, and Cl_3CCN^-, were not used in the calibration. In the case of the two fragment ions, the absence of reliable values for the BDEs precludes a realistic estimate of electron affinities but their thresholds may be used to deduce new information for the quantity (BDE − EA) and these are shown in Table 1. For the parent ion, where no molecular bond is broken, the threshold relation of eq 2 simplifies to $E_{th} \geq$ IP − EA and EA is estimated to be ≥0.3 eV. The uncertainty in the values deduced from the thresholds could be as high as 0.2 eV as noted above.

Steric Asymmetry. The steric asymmetry factors for the various ions formed in the electron transfer from potassium to CCl_3CN are shown in Figures 10−14. In each case, the steric asymmetry factors are compared with those for the major ion, Cl^-. Figure 10 clearly shows that the steric asymmetry for Cl^- and for CN^- is completely different: CN^- prefers negative-

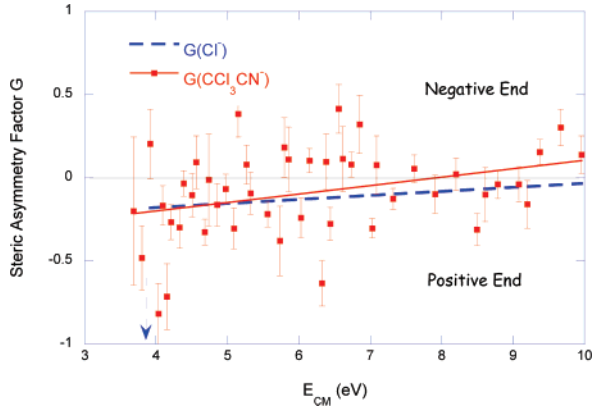

Figure 11. Steric asymmetry factor for the parent negative ion, CCl_3CN^- compared to the fit for Cl^-. Lines are linear least-square fits.

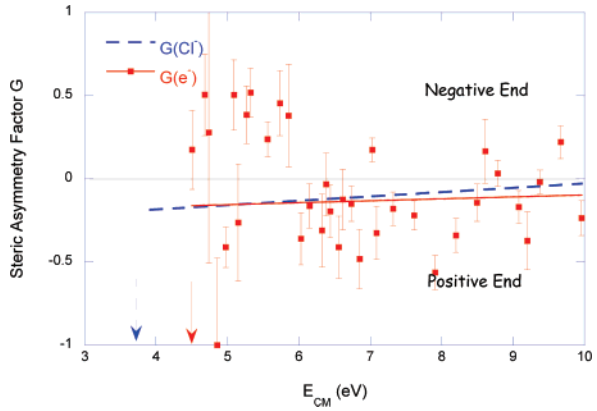

Figure 12. Steric asymmetry factor for autodetachment of electron with linear least square fit compared to fit for Cl^- data (dashed).

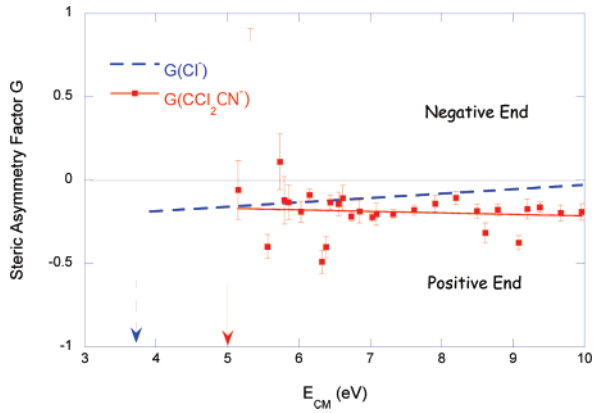

Figure 13. Steric asymmetry factor for CCl_2CN^- with linear least-square fit compared to fit for Cl^- data (dashed).

end (CN-end) attack whereas Cl^- slightly prefers positive-end (CCl_3-end) attack. The steric asymmetry factor for CH_3CN from Figure 5 is also plotted in Figure 10. Obviously the CN^- steric asymmetry factors are significantly different for the two molecules. The steric asymmetry for Cl^- is not only larger than that for CN^- from acetonitrile but also shows a distinct energy dependence, and suggests that Cl^- is likely to be formed by CCl_3-end attack collisions.

Because of the smaller signals involved, less definitive conclusions can be reached with respect to the other ions formed. Figures 11 and 12 suggest that the free electron and the parent negative ion, CCl_3CN^- have very similar steric asymmetry

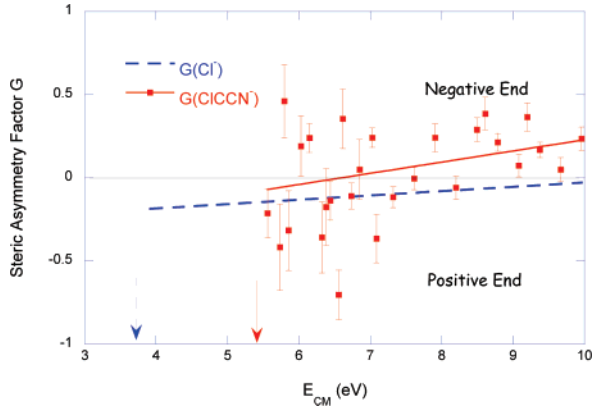

Figure 14. Steric asymmetry factor for $ClCCN^-$ with linear least-square fit compared to fit for Cl^- data (dashed).

factors possibly arising from a common precursor. Figures 13 and 14 show that CCl_2CN^- and $CClCN^-$ have different steric asymmetry factors from Cl^- at higher energies, even though all of these ions involve rupture of the C−Cl bond.

4. Discussion

CH_3CN/CH_3NC. Acetonitrile and methylisocyanide behave similarly. Figures 5 and 6 show that while the molecular orientation has a large effect on the production of the cyanomethyl anion, CH_2CN^-, it has virtually no effect on the formation of the CN^- anion, the major product following electron transfer. The steric asymmetry factor for CN^-, $G(CN^-) = 0.05$ and is *independent* of energy. It is *not* zero and reaction is only slightly favored by approaching the CN end of the molecule. In contrast, the steric asymmetry for CH_2CN^- depends on energy and favors approaching the CH_3 end of the molecule. Hydride ions, H^-, are formed, but in concentrations too low to evaluate the steric asymmetry. The parent negative ion, CH_3CN^-, is apparently not formed nor is the electron as we have observed in CH_3NO_2,[29,30] t-butyl Br,[15,16] and CCl_3CN.

In our preliminary report[22] we concluded that CH_2CN^- was formed by attack at the CH_3 end of the molecule but we were unable to rule out the importance of sideways attack in forming CN^-. Whereas steric asymmetry factors for electron transfer into the σ^* LUMO's found in saturated species such as CH_3Br tend to be large and strongly energy dependent, the steric asymmetry factor for electron transfer into the π^* orbital of CH_3NO_2 was very small and essentially energy independent. Because of the very small, energy independent G(CN), we now believe that formation of CN^- from CH_3CN or CH_3NC is favored by *sideways* attack, with the electron being transferred into the π^*_{CN} LUMO. Similar behavior was observed in transfer to the π^*_{NO} orbital in CH_3NO_2.[29,30]

A variety of experimental and theoretical evidence shows that the 3e π^*_{CN} orbital is the LUMO in CH_3CN.[31] Photoelectron spectra characterize the occupied orbitals and different electron bombardment experiments interrogate the unoccupied orbitals. These experiments with *free* electrons include the following: (a) The overall transmission of a beam of energy selected

(29) Brooks, P. R.; Harland, P. W.; Redden, C. E. *J. Phys. Chem. A* **2006**, *110*, 4697−4701.
(30) Brooks, P. R.; Harland, P. W.; Redden, C. E. *J. Am. Chem. Soc.* **2006**, *128*, 4773−4778.
(31) Jorgensen, W. L.; Salem, L. *The organic chemist's book of orbitals*; Academic Press: New York, 1973.

electrons reveals "resonances" in the cross section for transmission corresponding to transient states in the (electron + molecule) continuum. Measuring the energies of these resonances determines the vertical attachment energy of the transient negative ion, and the width of the resonance gives information about the lifetime of the transient negative ion via the uncertainty principle.[32−34] (b) Transient negative ions are unstable and can decay by autodetaching an electron, with, perhaps, an energy different from the incident energy because the electrons have excited a vibration of the neutral molecule. Careful measurement of the energy loss of the electrons thus gives information about which vibrational modes have been excited.[35] (c) The (energized) transient negative ion can decompose to give daughter ions, and identifying the ions and determining their energy dependence helps understand the fate of the excited transient negative ion.[19,20]

For acetonitrile (and somewhat similarly for methyl isocyanide), electron transmission measurements show broad resonances near 2.9 and 6.7 eV.[33,34,36,37] The resonance near 2.9 eV is similar to that in HCN and is attributed to capture into the doubly degenerate π^*_{CN} orbital. Electron energy loss spectroscopy at the 2.9 eV π^* resonance shows excitation of the ν_2 (C≡N stretch) and ν_8 (C−C≡N bend) vibrations, whereas at the 6.7 eV σ^* resonance the spectra are dominated by CH stretching modes, nicely corroborating molecular orbital predictions that the LUMO is 3e (π^*_{CN}) and the LUMO+1 is the $8a_1$ σ^* orbital.[34]

Dissociative attachment of *free* electrons also supports resonances near 3 and 6 eV, producing at low energy (in order of abundance) CH_2CN^-, $CHCN^-$, and CN^-. The CN^- signal is only about 1% of the CH_2CN^- signal at low energies[19,20] in contrast to the present experiments where CN^- is about 100× the CH_2CN^- signal. MNDO calculations for the radical anions for various saturated nitriles show that the HOMO (for the *anion*) is the antibonding π^*_{CN} orbital with the excess charge centered on the CN. Formation of ground state CN^- ($^1\Sigma$) requires that the π^* electron move to the σ^*_{CC} orbital which could occur via a predissociation where the Π and Σ curves cross as suggested in Figure 15.

From these theoretical and experimental observations we believe that the following picture emerges for low-energy electron transfer: Electrons are attached to CH_3CN by entering the π^*_{CN} orbital in the ground state geometry to give a transient negative ion of Π symmetry. This state lies in the electron−molecule continuum, being unstable with respect to autodetachment and having lifetime ≈ femtoseconds. To form CN^-, the Π state must live long enough to predissociate to the Σ state and the rapid autodetachment of the electron makes this unlikely. This accounts for the low yield of CN^- in the dissociative attachment experiments using free electrons. In the present experiments, however, the electron is not free, but is transferred from a potassium atom, and this significantly changes the simple picture painted above. Our previous experiments using different

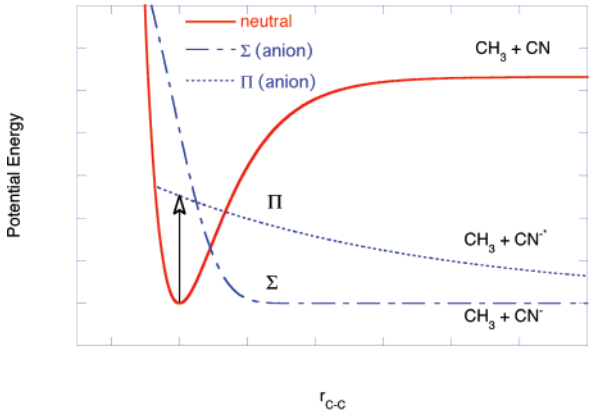

Figure 15. Highly schematic potential curves for CH_3CN, suggesting that vertical (Franck-Condon) attachment of an electron would produce a transient negative ion in a Π state evolving to excited CN^-. A collision-enhanced predissociation from the Π state to the Σ state is necessary to give ground state CN^-.

alkali metal atoms show that different donor atoms markedly affect not only the steric asymmetry but also the products formed.[18] The potassium atom could induce a bending in the molecule as we have seen in the case of CH_3NO_2[29]and affect the initial transfer or simply enhance the probability of the Σ−Π predissociation (Clark and Coulson proposed a similar mechanism for electron attachment in halobenzenes and noted that since a third body was involved a pressure dependence might be observed[38]). The K atom could also be considered to quench the formation of H_2CCN^- by opening the channel to the formation of CN^-. Theoretical work[39] also suggests that the K atom plays an important role in the process.

In summary, in the present electron-transfer experiments the steric asymmetry of the CN^- is nearly zero and is energy independent. This is not typical of alkyl halides, and CN is not simply a "super halogen." The electron-transfer experiments produce CN^- in attack of the K atom "sideways" to the axis of the CH_3CN molecule. The electron is transferred to the π^*_{CN} orbital to produce a Π transient negative ion and interaction between the incipient CH_3CN^- and K^+ enhances the curve crossing to the Σ state producing more CN^- than would be produced in the absence of the atomic interaction. (In the free electron experiments, the Σ−Π transition is not facilitated, and CN^- is far less likely to be formed.) The cyanomethyl anion, CH_2CN^- is preferentially produced in CH_3-end attack, with the electron being transferred into the σ^* LUMO+1. The large dipole moment for CH_3CN supports a dipole-bound state with a binding energy of ∼12 meV,[40] but the interaction between the nascent ions is apparently sufficiently large that we see no steric evidence for their participation.

CCl_3CN. The dominant signal from CCl_3CN is from Cl^- (even accounting for the fact that there are 3 Cl's). Gaussian calculations showed that the LUMO for this molecule had changed to an orbital with σ^*_{CCl} character, and the steric asymmetry strongly resembles that from chloroform measured earlier.[17]

The CN^- signal from CCl_3CN shows a much larger steric asymmetry than does CN^- from CH_3CN, due partly to the better

(32) Schulz, G. J. *Rev. Mod. Phys.* **1973**, *43*, 423−486.
(33) Burrow, P. D.; Howard, A. E.; Johnston, A. R.; Jordan, K. D. *J. Phys. Chem.* **1992**, *96*, 7570−7578.
(34) Edard, F.; Hitchcock, A. P.; Tronc, M. *J. Phys. Chem.* **1990**, *94*, 2768−2774.
(35) Edard, F.; Tronc, M. *J. Phys. B: At. Mol. Phys* **1987**, *20*, L265−L269.
(36) Jordan, K. D.; Burrow, P. D. *Acc. Chem. Res.* **1978**, *11*, 341−347.
(37) Hitchcock, A. P.; Tronc, M.; Modelli, A. *J. Phys. Chem.* **1989**, *93*, 3068−3077.
(38) Clarke, D. D.; Coulson, C. A. *J. Chem. Soc. A* **1969**, *1969*, 169−172.
(39) Maclagan, R. G. A. R. *Chem. Phys. Lett.* **2003**, *373*, 586−590.
(40) Hammer, N. I.; Diri, K.; Jordan, K. D.; Desfrancois, C.; Compton, R. N. *J. Chem. Phys.* **2003**, *119*, 3650−3660.

Table 2. $HV_{ON}-HV_{OFF}$ Legendre Coefficients

	a_1	a_2	a_3	R	<cos θ>
CH_3CN	−.456	−.076	−.076	.9986	−0.304
CH_3NC	−.469	−.067	−.071	.9986	−0.313
CCl_3CN	−.723	0.111	0.027	.99995	−0.48
CCl_3H	−.846	0.232	0.016	.99996	−0.56

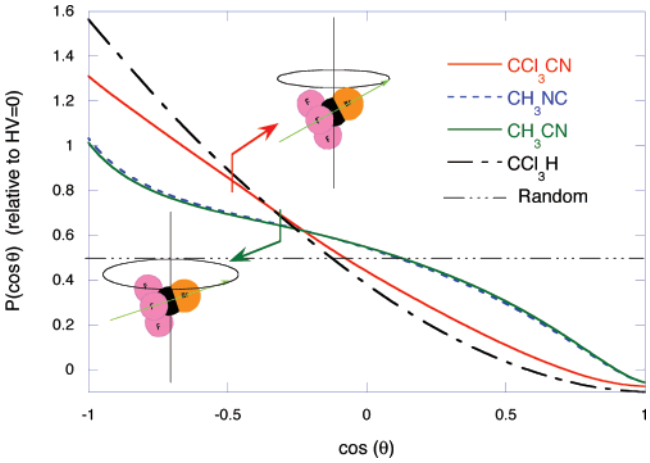

Figure 16. Quantum probability distribution P(cos θ) vs cos θ calculated for $HV_{ON}-HV_{OFF}$ using apparatus geometry and molecular constants. Horizontal dash-dot line is for a random beam. The average cos θ for CCl_3CN and CH_3CN are indicated by vertical bars with sketches of molecules with that orientation.

orientation of the molecule. Deflection in the inhomogeneous hexapole electric field favors molecules having values of cos θ = MK/[J(J+1)] near 1, requiring M, K ≈ J. But the rotational energy of a symmetric top molecule depends on K through the relation[26]

$$E_{rot} = BhJ(J+1) + (C-B)hK^2 \quad K = J, J-1, \cdots, -J$$

where the rotational constants are $B = h/(8\pi^2 I_B)$ and $C = h/(8\pi^2 I_C)$ and $I_{C,B}$ are the moments of inertia about the unique (C_3) axis of rotation and about an axis perpendicular to the C_3 axis. High orientation thus requires rotational states with K ≈ J which is favored by Boltzmann statistics if B > C, ($I_C > I_B$) [an oblate top] as exemplified by a bicycle wheel spinning about its axis. If C > B, [a prolate top] as exemplified by a pencil spinning about its axis (or CH_3CN)high values of K are not favored by Boltzmann statistics. Thus it is much easier to spin CCl_3CN about its axis than it is to spin CH_3CN about its axis, and the distribution of orientations, P(cos θ), in our oriented beams is quite different between the two molecules. We have calculated P(cos θ) for the present molecules and for CCl_3H for comparison using a procedure discussed elsewhere.[16] This distribution can be characterized using a fourth-order Legendre polynomial fit

$$P(\cos\theta) = \sum_0^3 a_i P_i(\cos\vartheta)$$

where $P_i(\cos\vartheta)$ are the Legendre polynomials and $a_0 = 0.5$. The coefficients a_i are listed in Table 2 for the $HV_{ON}-HV_{OFF}$ distribution together with <cos θ>. As the molecules become less prolate, higher values of K are populated and the molecules are better oriented.

It is important to realize that the angle θ is the angle between the rotationally averaged dipole moment and the *extant* electric field so the probability distribution P(cos θ) in the lab is the *same* for positive and negative attack orientations. The K atom explores the *same* distribution from different directions because the electric field is parallel to the K atom velocity in the negative-end attack orientation and antiparallel in the positive-end attack orientation.

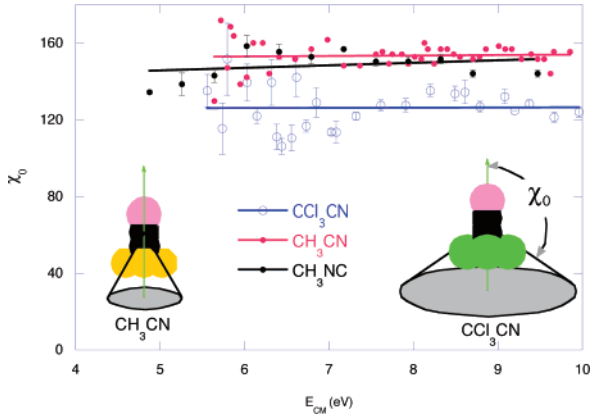

Figure 17. Half angle of cone of acceptance for forming CN^- from CH_3CN, CH_3NC, and CCl_3CN. χ_0 is measured from CN end, and lines are least-square fits.

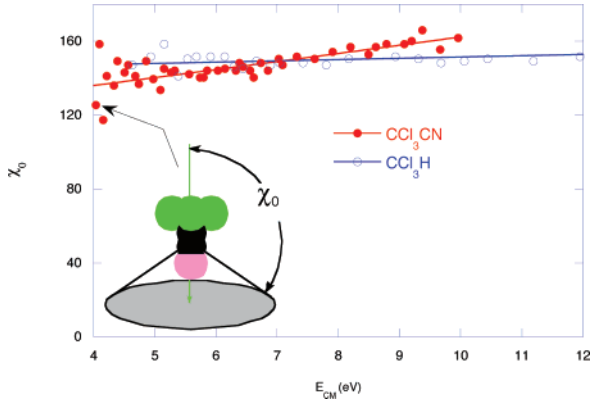

Figure 18. Half angle of cone of acceptance for forming Cl^- from CCl_3CN and CCl_3H. χ_0 is measured from Cl_3 end. Lines are least-square fits.

We have used a simple cone-of-acceptance model to account for the different orientation distributions where the reaction probability is assumed to be one for attack angles less than some critical value, χ_0, and zero otherwise.[16] Integrating this model over the positive and negative attack orientations and comparing with the steric asymmetry factor gives χ_0 for each energy. The values obtained are shown in Figures 17 and 18 for CN^- and Cl^- formation, respectively, together with sketches roughly indicating the different half angles. The allowed angles for CH_3CN and CH_3NC are about the same, ~155°, showing that any angle of attack is productive except for a 25° half-angle cone at the CH_3 end. This cone apparently arises from some hard barrier since increasing the collision energy fails to overcome it. The cone of acceptance for producing CN^- from trichloroacetonitrile is significantly smaller, ≈ 125°. The cone-of-acceptance for producing Cl^- from CCl_3CN is also large, ≥125° (but there are three Cl atoms!) and this cone clearly becomes larger as the energy increases. Reaction to form Cl^- occurs in a very large cone-of-acceptance at the CCl_3 end for both CCl_3CN and CCl_3H.

5. Summary

Electron transfer from potassium atoms to beams of oriented CH_3CN, CH_3NC and CCl_3CN gives K^+ and various negative ions that are identified by coincidence time-of-flight mass spectrometry. The dominant ion from CCl_3CN is Cl^-. All species produce CN^- (although its formation from CCl_3CN is severely depressed in favor of Cl^-) CX_2CN^- (X = H or Cl) and small amounts of other ions. CCl_3CN produces a parent negative ion, CCl_3CN^- and ions corresponding to the removal of one or two chlorine atoms from the parent negative ion, CCl_2CN^- and $CClCN^-$. The quantities (BDE − EA) for CCl_2CN^- and $CClCN^-$ are estimated to be ≤ 0.6 and ≤ 1.0 eV, respectively, and the electron affinity of the molecular ion CCl_3CN^- is estimated to be ≥ 0.3 eV.

The steric asymmetry factors for CN^- from the methyl compounds are similar, energy independent and very close to zero, ever so slightly favoring the negative CN end of the molecule. This seems to be a signature of molecules that prefer sideways attack and we conclude that the electron is accepted into the π_{CN}* LUMO. A cone-of-acceptance model suggests that all angles of attack are successful in initiating reaction except for a small cone-of-exclusion of half angle ~25° at the CH_3 end of the molecule. The steric asymmetry factor for CH_2CN^- strongly favors the positive CH_3 end and the absolute value becomes larger as the energy is decreased toward threshold, consistent with electron transfer into a σ* orbital at the CH_3 end of the molecule.

The steric asymmetry factor for CN^- from CCl_3CN is slightly larger (and noisier), favoring the negative end of the molecule. A cone of exclusion at the CCl_3 end appears to have a half angle ~55°. The dominant Cl^- ion is formed in attack of the σ_{CCl}* LUMO at the positive end of the molecule, and these steric preferences confirm that the CN end of the molecule is still negative as would be predicted by dipole vector addition.

Acknowledgment. This work is partially supported by the National Science Foundation under Grant No. 041149. Acknowledgment is made to the Donors of the American Chemical Society Petroleum Research Fund for partial support of this research.

JA074302D